

Effects of Filler Metal Composition on Joining Properties of Alloy 800H Weldments

SHIH-MING KUO, MING-YEN LI and CHIEN-LIN LAI

*New Materials Research & Development Department
China Steel Corporation*

The influences of filler metal composition on the microstructure, mechanical properties and corrosion resistance of Alloy 800H weldments were investigated. Three filler metals including Inconel 625 (60%Ni-21%Cr-9%Mo), Inconel 82 (72%Ni-17%Cr-2%Nb) and Alloy 309 (62%Fe-22%Cr-15%Ni) were used. Microscopic examination of the base materials, fusion zones and interfaces was characterized by using an optical microscope (OM), scanning electron microscope (SEM) and electron probe micro-analysis (EPMA). The results revealed precipitates of TiN with cuboidal morphology in the austenitic matrix along the grain boundaries of the Alloy 800H base metals. The thickness of unmixed zone formed at the Inconel filler metal/800H interface was much thinner than that at the Alloy 309/800H interface after welding. The formation of the unmixed zone with the different concentration gradients of the Ni, Cr and Fe elements was observed at the Alloy 800H/weld metal interface owing to the diffusion of nickel and iron during the re-solidification. The weldments made with the Inconel filler materials exhibited much higher strength and better ductility than iron-base Alloy 309 weld metal at room temperature. Inconel 625 exhibited the highest corrosion resistance among all tested filler metals and offered the optimum mechanical properties for Alloy 800H weldments.

Keywords: Alloy 800H, Microstructure, Mechanical property, Corrosion resistance

1. INTRODUCTION

The Alloy 800H is a fully austenitic Fe-Cr-Ni alloy (also commonly known as Incoloy 800H) often used in applications that require a combination of high-temperature strength and corrosion resistance. The alloy has been used extensively by the petrochemical and nuclear power industries for steam-naphtha reformers and superheater/reheater tubes, respectively. Since all these applications require welding as a fabrication step, the Alloy 800H base metal must be resistant to hot cracking during welding and ultimately must exhibit as-welded properties that will ensure extended service life in severe mechanical/environmental conditions. The selection of a proper filler metal in dissimilar welding is one of the most challenging factors in high temperature environments like petrochemical industries. The filler metal chemistry should match with the major elements of the base metal chemistry. These elements are primarily nickel and chromium, but the filler metals available typically contain the other elements, also forming an undesirable composition in the weld zone. An extensive literature review was conducted in order to get a clear picture of the work done in the past in relation to this work to find suitable filler materials in welding processes⁽¹⁻⁵⁾. However, most of the investigations were focused on the

effect of processing parameters and fillers chemistry on the microstructure and weldability of dissimilar welds between stainless steel and nickel base alloys. Few comments were made relating to the interfacial behavior between filler metal and Alloy 800H during the welding process. The present investigation is concerned with the Alloy 800H weldment and the objective aims to select the most appropriate filler material based on a comparative evaluation of three filler metals (Inconel 625, Alloy 309 and Inconel 82). The effect of filler metal composition on the microstructure characterization, mechanical properties and corrosion resistance of Alloy 800H weldments has also been studied.

2. EXPERIMENTAL METHOD

The base metal, Alloy 800H, was produced by CHINA STEEL CORPORATION, Kaohsiung, Taiwan, in plate form with dimensions 150 x 150 x 6 mm³. Three filler metals including Inconel 625, Alloy 309 and Inconel 82 were used as filler metal with a diameter of 2.4 mm. The chemical compositions of the base and filler materials are given in Table 1. The specimens were machined to make a single V groove butt joint configuration with 80° groove angle and the root face and root opening were 1.0 mm and 2.4 mm respectively. Welding

procedure was performed in four passes by the gas tungsten arc welding process with direct current electrode negative. The completed welds were tested by X-radiography to examine the specimens after welding; thereby ensuring no defects occurred that could affect mechanical test results.

The microstructure of the specimen was characterized by OM (Optical Microscope), SEM (Scanning Electron Microscopy ; JEOL JSM-7000F), EDX (Energy Dispersive X-ray spectrometer) and EPMA (Electron Probe Micro-Analysis ; JEOL JXA-8900R). All specimens prior to SEM and EPMA examinations were mechanically polished with wet SiC abrasive paper down to 1 μm roughness and then chemically etched at room temperature in 30 cc HCl, 30 cc HNO₃ and 20 cc H₂O solution for 1 minute.

The flat uniaxial tensile specimens were prepared with the cross-sectional area of 6 x 12 mm² (gage length of 50 mm) and 4 x 6 mm² (gage length of 25 mm) for room temperature and 925°C longitudinal tensile testing, respectively. These specimens were cut from the weldments with the cutting axis length perpendicular to the weld fusion line and mechanically ground by 1500 grit

SiC abrasives. Transverse tensile specimens (rolling direction of Alloy 800H plate perpendicular to welding direction) were also produced and tested both at room temperature and at 925°C. Fractographs of ruptured specimens after tensile testing were examined by SEM. In addition, average hardness measurements were made across the weld metals at a load of 200g using a Vickers hardness tester.

For corrosion testing (ferric chloride pitting testing), the samples with sufficient weld metal cross-section were mechanically polished, then at 22°C for 72h in 6.0 wt% FeCl₃ solution. The corrosion rates of welds produced with different filler materials were determined by calculating the weight loss of the specimen after ferric chloride pitting testing.

3. RESULTS AND DISCUSSION

3.1 Base metal microstructures

3.1.1. Alloy 800H base metal

Alloy 800H is a solid solution-strengthened iron–nickel base superalloy. Figure 1(a) shows that the microstructure of solution annealed Alloy 800H with the fully

Table 1 Chemical composition of materials used (wt%)

Element	Base materials		Undiluted filler materials	
	Alloy 800H	Alloy 625	309	Alloy 82
C	0.06	0.01	0.04	0.02
Si	0.4	0.1	0.37	0.1
Mn	0.6	0.01	1.35	2.8
Ni	31.5	60.8	14.5	72.1
Cr	21.2	20.8	21.6	16.5
Mo	-	8.9	0.1	-
Ti	0.24	0.3	-	-
Nb	-	3.5	-	2.2
Fe	Balance	Balance	Balance	Balance

(correction to spacing and layout)

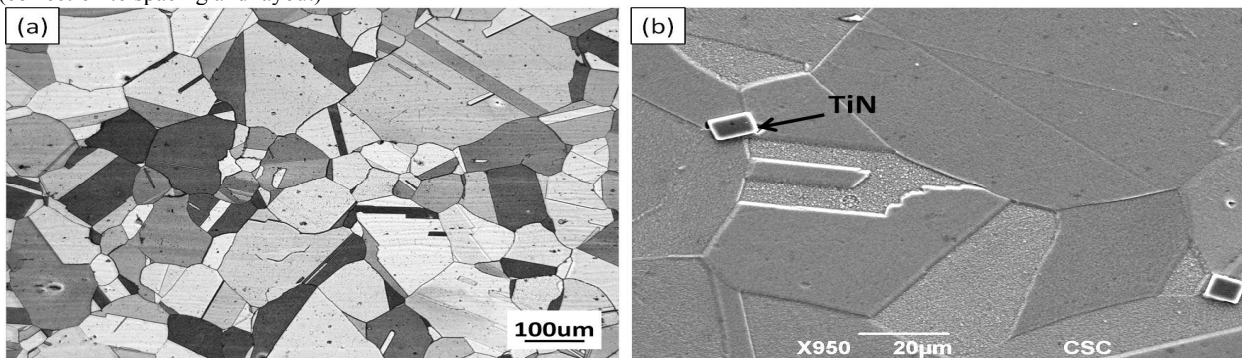


Fig.1. (a) Optical microstructure of Alloy 800H and (b) SEM image of precipitate particle in Alloy 800H base material.

austenitic matrix containing several annealing twins across the grains can be observed in the microstructure formed by stress relieving after cold working, which is surrounded by fine grains. The coarse grain size (100 to 150 μm) of Alloy 800H possesses outstanding high-temperature mechanical properties and resistance to creep. Alloy 800H contains 0.36% titanium and 0.09% carbon and hence has a tendency to form titanium carbide and titanium carbonitride during high temperature exposure because they do not dissolve easily during solution annealing even if high soaking temperatures are employed⁽⁶⁾. These particles provide coherency strengthening to the matrix and enhance the fracture toughness of the material. The precipitated phase with cuboidal morphology shown in austenite matrix and along the grain boundary is primary titanium nitrides, TiN, as identified with EDX and shown in Figure 1(b).

3.2 Weld metal microstructures

3.2.1. Inconel 625 weld metal

Figure 2(a) illustrates that the weld metal microstructure of the Inconel 625 exhibits austenitic structure with a dendritic morphology. Migration grain boundaries (MGBs) are mostly prevalent in fully austenitic weld metals, precipitates form along the solidification sub-grain boundaries (SSGBs) and solidification grain boundaries (SGBs). These precipitates are rather effective in “pinning” the crystallographic component of the SGBs. Therefore, they prevent it from migrating away from the parent SGB⁽⁷⁾. It is known that the partition coefficient of Mo decreases as the iron content in the weld increases. Figure 2(a, b) shows the SEM micrograph of Inconel 625 weld metal, which consisted of fine dendrites with the high concentration of Mo according to the EDX analysis results (Figure 2(c, d)).

3.2.2. Alloy 309 weld metal

The microstructure of the Alloy 309 weld metal is shown in Figure 3(a, b). This reveals a primary ferrite structure with a dendritic morphology showing well-

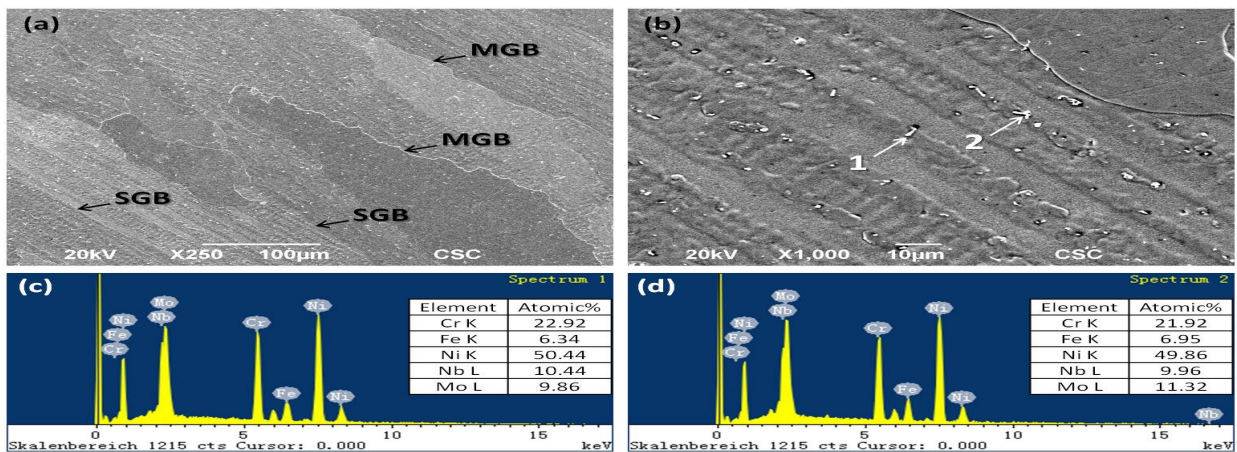


Fig.2. (a) Microstructure of Inconel 625 weld metal, (b) High magnification micrograph of Fig.2(a) and (c) · (d) EDX analysis of the fine dendrite region in Fig.2(b).

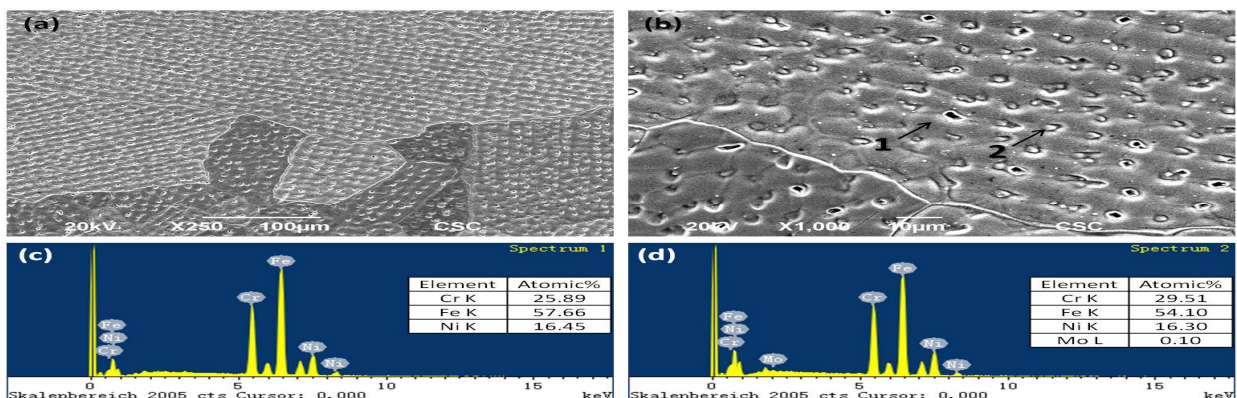


Fig.3. (a) Microstructure of Alloy 309 weld metal, (b) High magnification micrograph of Fig.3(a), (c) EDX analysis of the inter-dendrite region in Fig.3(b) and (d) EDX analysis of the dendrite region in Fig.3(b).

developed side-branches. Similar composition was identified in the dendrites and the inter-dendrite regions, but the dendrites with the higher chromium content were found in the EDX analysis (Figure 3(c, d)) of this weld metal. It is known that dendritic structures are associated with a greater degree of segregation and are more prone to cracking⁽⁷⁾. In the case of the Inconel 82 and Inconel 182 weld metals, mechanical property evaluation of the fusion zones showed that the Inconel 82 welds displayed a consistently higher tensile elongation and Charpy impact toughness when compared to the Inconel 182 weld metal.

3.2.3. Inconel 82 weld metal

The weld metal Inconel 82 contains dendrite and inter-dendritic zones as shown in Figure 4(a). The microstructures of the Inconel weld metal are fully austenitic, due to the presence of Nb; the extent is stabilized at a high temperature. In addition, the solidification mode is changed from cellular to dendritic because Nb has an intense tendency to increase the degree of constitutional under-cooling⁽⁷⁻⁹⁾. The microstructures of weld metals are similar to an extensive migrated grain boundary⁽¹⁰⁾. The MGBs carry a high angle mis-orientation of the parent solidification grain boundary. The driving force of

their migration is the same as simple grain growth in the base metal. It is also possible that some segregation might occur along the MGBs, possibly due to a “sweeping” mechanism⁽⁷⁾. Core and fine dendrite were identified with SEM image of this weld metal as shown in Figure 4(b), which was composed of fine dendrites with the high concentration of Nb detected by EDX analysis of this weld metal (Figure 4(c, d)).

3.3 Interfacial microstructures

3.3.1. Interface between Inconel 625 weld metal and Alloy 800H

The interfacial regions of the Inconel 625 weldment and the Alloy 800H base metal are shown in Figure 5(a, b). From Figure 5(a), epitaxial growth at the fusion line was identified. The similarity of the crystal structure and the chemical composition between the base and weld metals have caused epitaxial growth to occur⁽¹¹⁾. The unmixed zone exists as a laminar layer where a small portion of the base metal has totally melted and resolidified without undergoing filler metal dilution. The melting point range of Inconel 625 weld metal (1290-1350 °C) is similar to the Alloy 800H base metal (1357-1385 °C), only a small fraction of the base metal can be melted

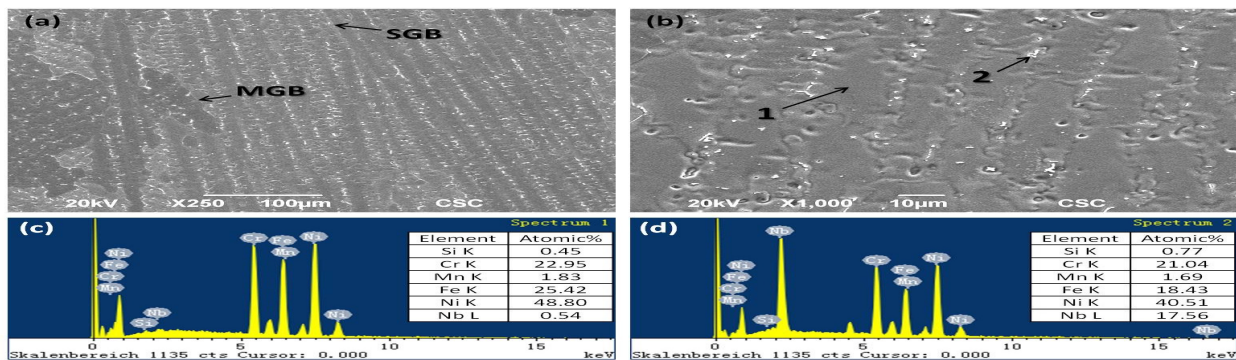


Fig.4. (a) Microstructure of Inconel 82 weld metal, (b) High magnification micrograph of Fig. 4(a), (c) EDX analysis of the inter-dendrite region in Fig.4(b) and (d) EDX analysis of the dendrite region in Fig.4(b).

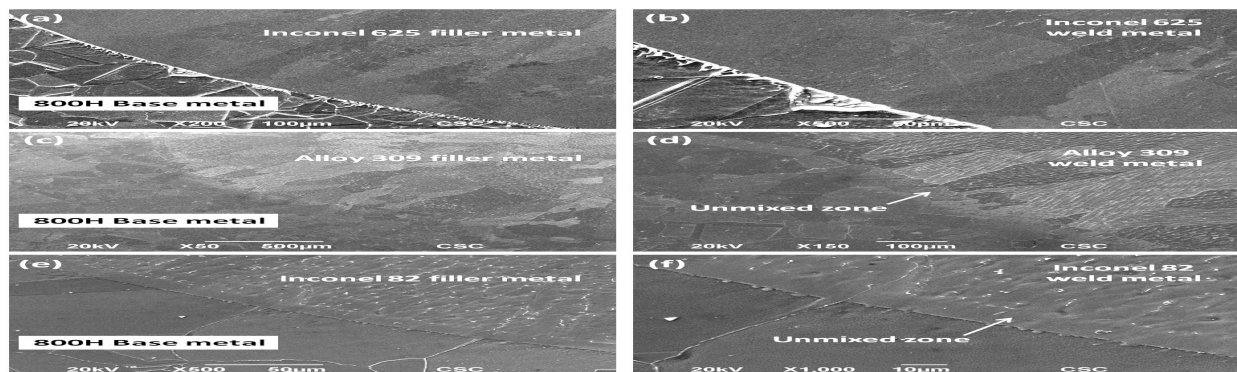


Fig.5. (a)-(b) Microstructure of interface between Inconel 625 weld metal and Alloy 800H : (c)-(d) Microstructure of interface between Alloy 309 weld metal and Alloy 800H : (e)-(f) Microstructure of interface between Inconel 82 weld metal and Alloy 800H.

and no dilution occurs in the re-solidification stage. Therefore, no obvious unmixed zone was observed at the interface between Inconel 625 weld metal and base metal in the higher magnification micrograph (Figure 5(b)).

3.3.2. Interface between Alloy 309 weld metal and Alloy 800H

The interface between Alloy 800H base metal and Alloy 309 weld metal is shown in Figure 5(c, d). The Alloy 309 weld metal exhibited a higher melting point (1399-1454 °C) than the base metal, so that much more fraction of the base metal melted and resolidified. An unmixed zone with the thickness of 60 µm was clearly observed at the filler metal/Alloy 800H interface in the higher magnification micrograph (Figure 5(d)). The Alloy 309 filler metal exhibited a higher melting point than Alloy 800 base metal, so that grain boundary melting and liquation was induced in the interface between Alloy 309 fusion zone and heat affected zone (HAZ) of Alloy 800. The partially melted zone in the Alloy 309 weld appears to be much wider than that of the Inconel 625 weld due to the higher melting point of the Alloy 309 filler. The original grain boundaries in many cases have moved to locations a few microns away from the previous sites. The tendency of grain boundaries to melt in alloy 800 HAZ was well known and is attributed to the enrichment of titanium at these boundaries⁽¹²⁾. Titanium at these boundaries not only lowered the melting point constitutionally but also formed the low melting carbide-austenite eutectics during solidification.

3.3.3. Interface between Inconel 82 weld metal and Alloy 800H

Figure 5(e) shows grain growth in the HAZ and near the interface of Alloy 800H. The interface of the Inconel 82 weld metal with Alloy 800H base metal (Figure 5(f)) shows the presence of an unmixed zone with the thickness of 15 µm. The thickness of the unmixed zone at the Inconel 82/800H interface is much thinner than that at the Alloy 309/800H interface. This may be attributed to the smaller compositional difference between the Inconel weld metal and the Alloy 800H base metal. Welds between widely dissimilar combinations are known to exhibit much wider unmixed or partially mixed zones where the microstructure and chemical composition are quite different from that of the surrounding weld metal⁽¹³⁾.

On the other hand, the melting point of the Alloy 800 base metal (1357-1385°C) is slightly higher than that of the Inconel 82 weld metal (1295-1339°C), and the convection currents are not able to promote adequate fluid flow and mixing. The Alloy 800 has a melting point as well as a composition closer to that of the Inconel weld metal. In this case, a wide unmixed zone cannot

form as convection in the weld puddle would ensure that only a thin laminar layer would remain unmixed. In addition, more grain growth occurred in the HAZ of the Alloy 800H base metal can be attributed to the temperature increase during various welding passes, as shown in Figure 5(e, f).

3.4 EPMA line-scan and elemental mapping analysis at the interface

3.4.1. EPMA analysis at the Inconel 625/ Alloy 800H interface

Figure 6 shows the EPMA line-scan analysis of the welds produced with different filler materials. Inconel 625 weld metal displayed the dendritic structure with the high concentration of carbon and niobium across weld zones (Figure 6(d)). Homogeneous composition was identified across weld zones and no significant diffusion of Ni, Fe, Cr, Nb and Mo into the unmixed zone was observed. The migration of elements across the weldments may be suppressed by the homogeneous distribution of molybdenum while using Inconel 625 as a filler wire. Figure 7 shows the EPMA elemental mapping of the interface between Inconel 625 weld metal and Alloy 800H. Also, rich amount of Mo content was identified in the NbC dendrites across weld zones. EPMA mapping results revealed that much higher Fe content was found near the Inconel 625/800H interface in weld zones due to diffusion of elements from weld metal to base metal. The formation of the unmixed zone with a different concentration gradient of the Ni, Cr and Fe elements was observed at the Inconel 625/800H interface owing to the diffusion of nickel and iron during the re-solidification, as shown in Figure 7.

3.4.2. EPMA analysis at the Alloy 309/ Alloy 800H interface

There was a small difference in concentration of Cr and Fe between the Alloy 309 weld metal and 800H base metal according to the EPMA line-scan result (Figure 6(e)). No enrichment of elements was observed at the interface between the Alloy 309 weld metal and base metal after the welding process. Homogeneous composition was identified across weld zones and no significant diffusion of Ni, Fe, Cr and Mo into the unmixed zone was observed, as seen in Figure 6(e).

A much wider unmixed zone at the interface between Alloy 309 weld metal and Alloy 800H was identified with the EPMA mapping result, as shown in Figure 8. Due to the diffusion of nickel and iron during the re-solidification of Alloy 800H, an unmixed zone with a concentration gradient of the Ni, Cr and Fe elements was formed at the Alloy 309/800H interface after the welding process.

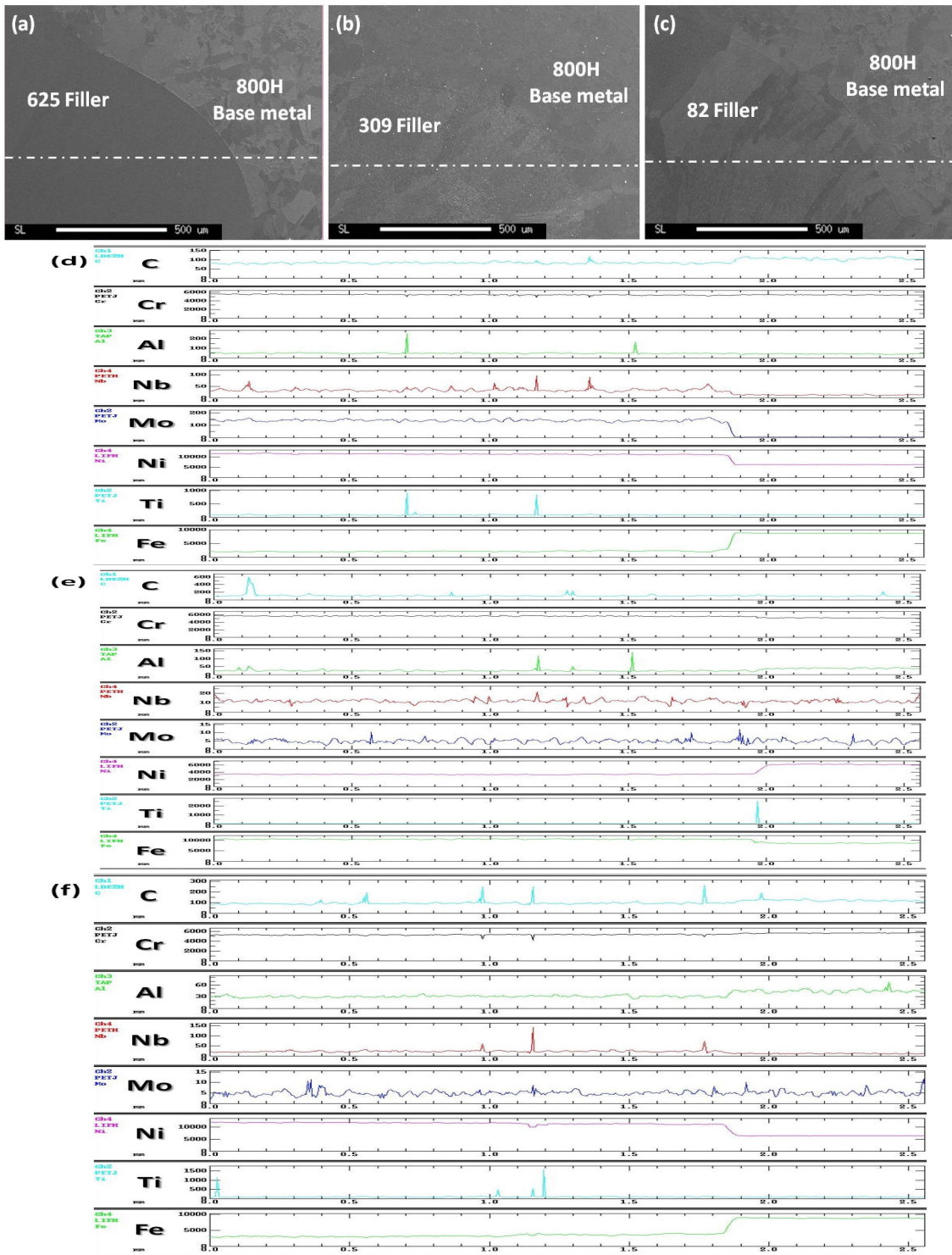


Fig.6. EPMA line-scan analysis for the welds produced with different filler materials : (a)-(c) SEM cross-sectional picture at the weld metal /Alloy 800H interface while using Inconel 625, Inconel 82 and Alloy 309 as filler metal respectively ; (d)-(f) EPMA line-scan analysis of C, Cr, Al, Nb, Mo, Ni, Ti, and Fe elements distribution profile in Fig.6(a)-(c).

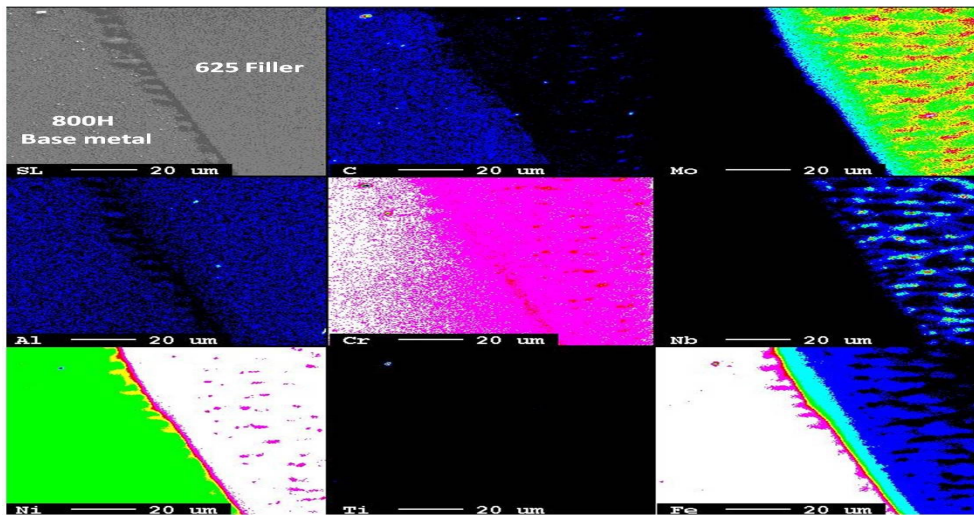


Fig.7. EPMA elemental mapping of interface between Inconel 625 weld metal and Alloy 800H.

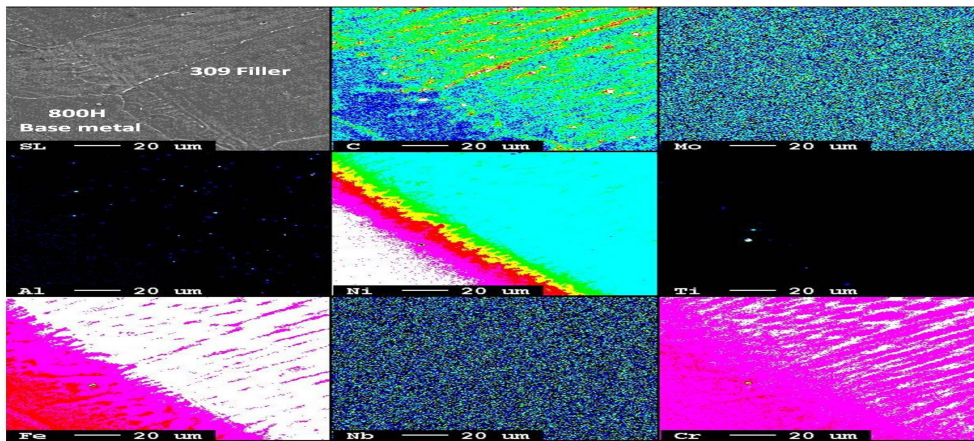


Fig.8. EPMA elemental mapping of interface between Alloy 309 weld metal and Alloy 800H.

3.4.3. EPMA analysis at the Inconel 82/ Alloy 800H interface

The clear differentiation of Ni and Fe compositions was observed in the interface region between the Inconel 82 and Alloy 800H base metal, as shown in Figure 6(f). Inconel 82 weld metal displayed the dendritic structure with the high concentration of carbon and niobium across weld zones. No enrichment of elements was observed at the interface between the Inconel 82 weld metal and base metal after the welding process. Homogeneous composition was identified across weld zones and no significant diffusion of Ni, Fe, Cr, Nb and Mo into the unmixed zone was observed. According to the EPMA mapping result, an unmixed zone with a concentration gradient of the Ni, Cr and Fe elements was identified at the interface between Inconel 82 weld metal and Alloy 800H, as seen in Figure 9.

3.5 Mechanical property tests

3.5.1. Hardness tests

The hardness variations across the welds with different filler materials are shown in Figure 10. The Inconel 625 weld exhibited a greater hardness (<205Hv) than those of the two base materials, which is similar to the hardness of Inconel 82 (<183Hv). However, the lower hardness of the Alloy 309 weld than those of the two base materials was determined due to the lower intrinsic mechanical strength of Alloy 309. In general, there is a positive correlation between hardness and strength; the higher the hardness value, the higher the strength. It is further found that in Inconel 82 weld there is a gradual, though slight, decrease in hardness in the weld metal on traversing from the Inconel 82 to the Alloy 800 side (Figure 10(c)). This suggests that despite the convection effects in the weld metal there could be a gradient in composition on account of dilution from the two different materials in the interface region. Thus, it was also observed that the small increase in hardness in

the weld metal traversing from the Alloy 309 to the Alloy 800 side. However, the similar hardness value in Inconel 625 weld was identified across the weld zone

due to the homogeneous distribution of molybdenum, as seen in Figure 10(c).

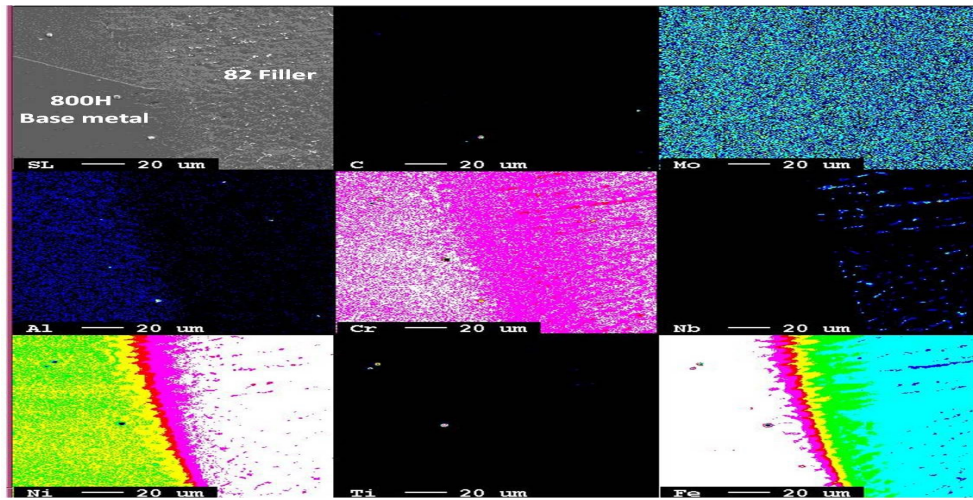


Fig.9. EPMA elemental mapping of interface between Inconel 82 weld metal and Alloy 800H.

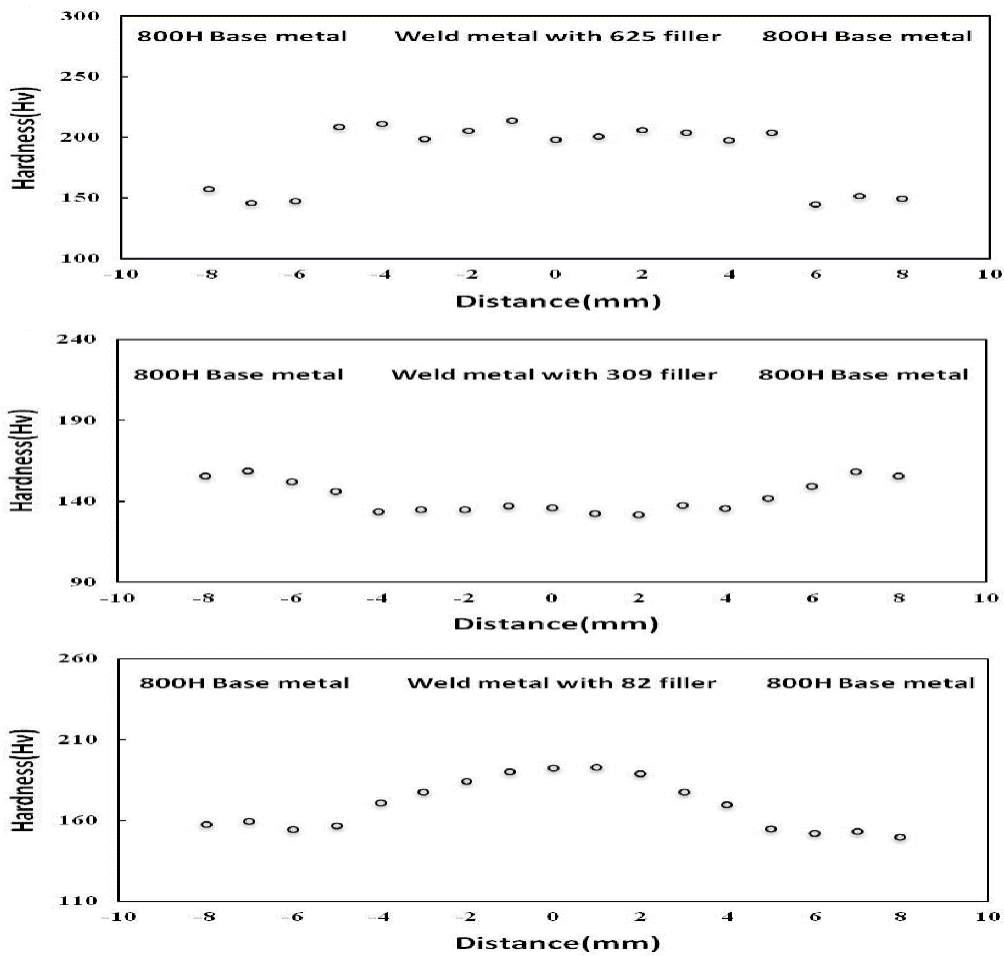


Fig.10. Hardness profile across the welds produced with different filler materials : (a) Inconel 625 weld metal ; (b) Alloy 309 weld metal and (c) Inconel 82 weld metal.

3.5.2. Tensile tests

Figure 11 illustrates the fractographic results of ruptured specimens after room temperature tensile testing. As can be seen, the Alloy 309 specimen ruptured at the fusion zone (FZ), whereas the Inconel 625&82 specimen ruptured at the base metal (BM). In Lee and Kuo's study of I-52 and I-82 weldments⁽¹⁴⁾, rupture location tendency did not vary with increasing number of welding passes, so a number of passes may be assumed to be an irrelevant factor. Similar tensile properties of the transverse (rolling direction of Alloy 800H plate perpendicular to welding direction) and longitudinal specimens made with three filler metals at room temperature were determined, as shown in Table 2. The Inconel 625 specimen has a higher tensile strength (567-583 MPa) and a greater elongation (40-41%), which is similar to the Inconel 82 data (tensile strength: 573-585 MPa, elongation: 38-40%). In comparison, the tensile strength

(547-550 MPa) and elongation (<30%) of the Alloy 309 specimen are lower. If the FZ strength is higher than the BM tensile strength, the rupture position will occur at the BM and the tensile strength and elongation will approach that of the BM. The superior weld joint strength of the Inconel 625&82 specimen could be attributed to its higher nickel content and solid solution strengthening of niobium and molybdenum. The SEM fractographs of ruptured specimens with different filler materials after room temperature tensile testing shows the dimple structure, while the joints made with these three filler metals indicating the ductile fracture, as shown in Figure 12. The specimens made with Inconel 625&82 fillers ruptured at the base metal exhibited more obvious dimple structure, resulting in the much higher elongation, as shown in Table 2.

Figure 13 shows the fractographic results of ruptured specimens after 925°C tensile testing. Similar



Fig.11. Ruptured specimens after tensile testing : (a) Inconel 625 weld metal, (b) Alloy 309 weld metal and (c) Inconel 82 weld metal.

Table 2 Tensile properties of transverse and longitudinal specimens at room temperature.

Filler metal	Testing direction	Ultimate tensile Strength (Mpa)	Yield Strength (Mpa)	Total elongation (%)	Location of failure
Inconel 625	Transverse	566.6	272.6	41.0	Base metal
Inconel 625	Longitudinal	582.7	280.8	40.2	Base metal
Alloy 309	Transverse	549.8	280.0	30.1	Weld metal
Alloy 309	Longitudinal	547.2	279.7	30.4	Weld metal
Inconel 82	Transverse	572.9	273.2	38.0	Base metal
Inconel 82	Longitudinal	584.5	284.6	39.7	Base metal

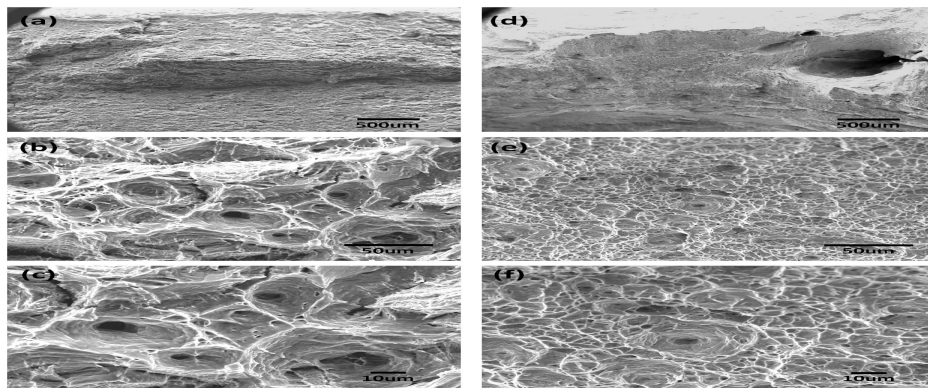


Fig.12. SEM fractographs of ruptured specimens after room temperature tensile testing : (a)-(c) Rupture occurred in Alloy 800H base metal and (d)-(f) Rupture occurred in Alloy 309 weld metal.

tensile properties of ultimate tensile strength and yield strength for all transverse and longitudinal tensile specimens in the high-temperature test were determined, as shown in Table 3. While the joints made with Alloy 309 filler material exhibited fusion zone failure, the weldments with Inconel 625 and Inconel 82 filler materials failed in the weaker base metal, i.e., Alloy 800H. The base metal failures exhibited a greater elongation than the weld metal failures. Regarding the tensile properties determined at 925°C, there is an understandable drop in ultimate tensile strength and yield strength in all cases. Concerning ductility, while there was no significant change in the tensile elongation in the case of weldments produced with the Inconel 82 fillers, a slight decrease in elongation was observed for the joints made with Inconel 625 and Alloy 309 filler materials. The SEM fractographs of ruptured specimens with different filler materials after 925°C tensile testing shows the dimple

structure, while the joints made with these three filler metals indicating the ductile fracture, as shown in Figure 14. Among these three filler materials, the Inconel 625&82 specimen exhibited much higher ductility so that the more obvious dimple structure was observed at the base metal after 925°C tensile, as seen in Figure 14.

3.6 Corrosion resistance test

According to ASTM G48 method A, the ferric chloride pitting test, i.e. a specimen at 22°C in a 6.0 wt% FeCl₃ solution for 72h, is quite useful for a quantitative standard for susceptibility to chloride ion corrosion. Herein it was used as a test of weld corrosion resistance. A more severe corrosion attack was observed in the Alloy 309 weld than that in the Inconel 625 (or Inconel 82) welds after ferric chloride pitting testing, as shown in Figure 15. The density of pitting holes may be used as the qualitative term to assess the corrosion attack. The

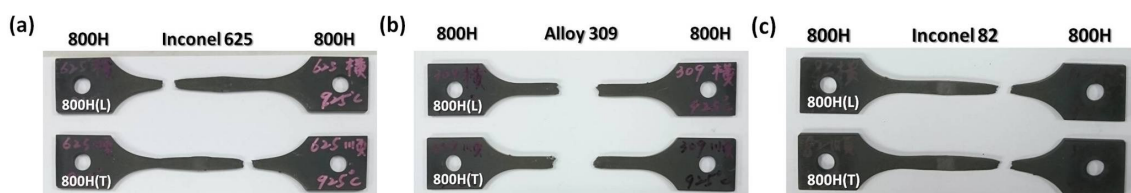


Fig.13. Ruptured specimens after 925°C tensile testing : (a) Inconel 625 weld metal ; (b) Alloy 309 weld metal and (c) Inconel 82 weld metal.

Table 3 Tensile properties of transverse and longitudinal specimens at 925°C.

Filler metal	Testing direction	Ultimate tensile Strength (Mpa)	Yield Strength (Mpa)	Total elongation (%)	Location of failure
Inconel 625	Transverse	102.5	74.3	35.6	Base metal
Inconel 625	Longitudinal	100.7	73.7	37.3	Base metal
Alloy 309	Transverse	100.3	73.5	27.5	Weld metal
Alloy 309	Longitudinal	99.1	73.4	27.2	Weld metal
Inconel 82	Transverse	101.4	72.8	37.6	Base metal
Inconel 82	Longitudinal	99.4	72.8	40.1	Base metal

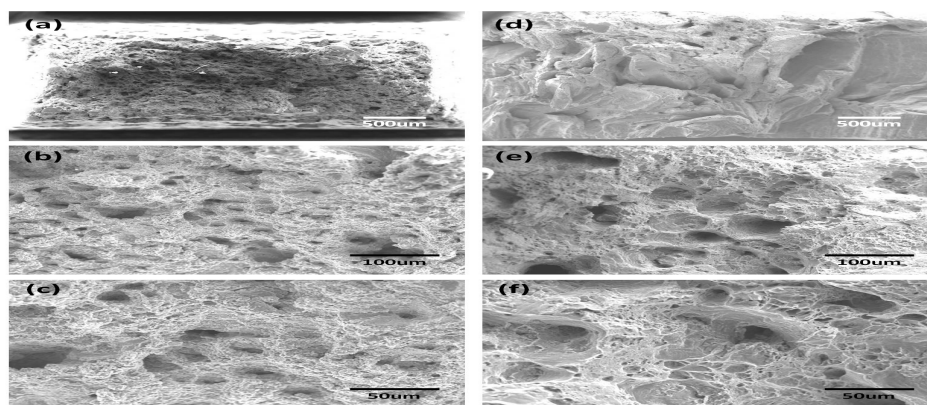


Fig.14. SEM fractographs of ruptured specimens after 925°C tensile testing : (a)-(c) Rupture occurred in Alloy 800H base metal and (d)-(f) Rupture occurred in Alloy 309 weld metal.

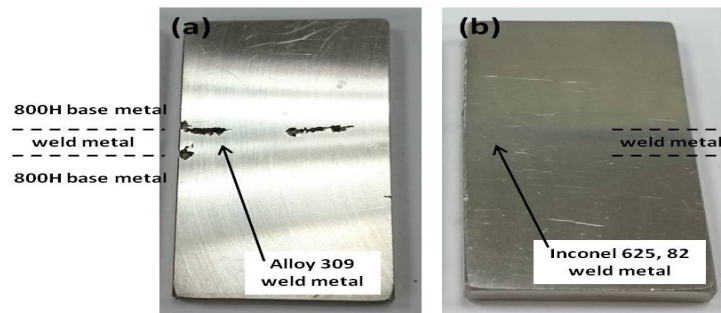


Fig.15. Corroded surface of welds produced with different filler materials after ferric chloride pitting testing for 72h in 6.0 wt% FeCl₃ solution : (a) Alloy 309 weld metal and (b) Inconel 625, 82 weld metal.

density of pitting holes in the Alloy 309 weld is apparently higher than that in the Inconel 625 (or Inconel 82) welds. Based on this fact, the corrosion resistance of the Inconel 625 (or Inconel 82) weld is believed to be better than that of the Alloy 309 weld. The quantitative evolution of the corrosion was determined by the weight loss measurement of the specimen after the test. The experimental results revealed that weight loss values are about 2.69 g/m² h, 3.38 g/m² h and 2.81 g/m² h respectively, for Inconel 625, Alloy 309 and Inconel 82 welds. The image of Figure 15(a) revealed the main corrosion sites (pitting holes) formed in the interface between Alloy 309 weld metal and Alloy 800H. The drop of Ni and Cr content in the unmixed regions is the important cause of low corrosion resistance in the Alloy 309/800H interfaces. Ni and Cr provide the major corrosion resistance for nickel-based alloy. Many studies have indicated that the lower levels of Ni and Cr can cause reduction of corrosion resistance to many corrosive aqueous media environments⁽¹⁵⁾. Their experimental results showed that the Intergranular corrosion resistance of x% Cr-60% Ni-Fe (balance) alloys increased with increasing Cr content up to about 30%. Similarly, for 30% Cr-x% Ni-Fe (balance) alloys, Ni also improved the Intergranular corrosion resistance with increasing Ni content up to about 60%. The Ni (60 wt.%) and Cr (30 wt.%) content in alloy 690 is designed in accordance with these results.

Since the Inconel 82 weld showed no Mo content while the Inconel 625 weld showed about 8.9 wt.%, the higher Mo content could be the main cause of increased corrosion resistance in the Inconel 625 weld. Therefore, the Inconel 625 weld exhibited the slowest corrosion rate among all tested filler metals. The beneficial effect of Mo addition on pitting corrosion resistance was discussed in many studies of stainless steels and nickel-based alloy^(2,6,15). An additional cause of corrosion would be the differential chemical composition of the unmixed zone relative to the filler and base metal regions, this difference tending to induce galvanic corrosion at the filler/base metal interface sites.

4. CONCLUSIONS

1. The precipitates of TiN with cuboidal morphology were observed in the austenitic matrix along the grain boundaries of the Alloy 800H base metals. Migration of grain boundaries in the Inconel 82 weld metal was very extensive when compared to that in Inconel 625 and Alloy 309 weldments.
2. The unmixed zone exists as a laminar layer where a small portion of the Alloy 800H base metal has totally melted and resolidified without undergoing filler metal dilution. The thickness of unmixed zone formed at the Inconel filler metal/800H interface was much thinner than that at the Alloy 309/800H interface after the welding process.
3. EPMA analysis shows that the formation of the unmixed zone with a different concentration gradient of the Ni, Cr and Fe elements at the Alloy 800H/weld metal interface was due to the diffusion of nickel and iron during the re-solidification.
4. Similar tensile properties of the transverse (rolling direction of Alloy 800H plate perpendicular to welding direction) and longitudinal specimens made with three filler metals at room temperature and elevated temperature (925°C) were determined. The weldments made with the Inconel filler materials exhibited much higher strength and ductility than iron-base Alloy 309 weld metal at room temperature.
5. Inconel 625 exhibited the highest corrosion resistance among all tested filler metals and offered the optimum mechanical properties for Alloy 800H weldments.

REFERENCES

1. H.T. Lee, S.L. Jeng, C.H. Yen, T.Y. Kuo: J. Nucl. Mater, 2004, vol. 335, pp. 59-69.
2. R. Dehmolaei, M. Shamanian, A. Kermanpur: Mater. Charact, 2008, vol. 59, pp. 1814-1817.
3. A.K. Bhaduri, I. Gowrisankar, V. Seetharaman, S. Venkadesan, P. Rodriguez: Mater. Sci. Technol,

- 1988, vol. 4, pp. 1020-1029.
4. A.K. Bhaduri, G. Srinivasan, T.P.S. Gill, S.L. Mannan: *Int. J. Press. Vessel. Pip.*, 1995, vol. 61, pp. 25-33.
 5. K.H. Song, W.Y. Kim, K. Nakata: *Mater. Des.*, 2012, vol. 35, pp. 126-132.
 6. R. Dehmolaie, M. Shamanian, A. Kermanpur: *Mater. Charact.*, 2008, vol. 59, pp. 1447-1454.
 7. W.F. Savage, C.D. Lundin, A.H. Aronson: *Weld. J.*, 1965, vol. 44, pp. 175s-181s.
 8. T.Y. Kuo, H.T. Lee: *Mater. Sci. Eng. A*, 2002, vol. A338, pp. 202-212.
 9. P.L. Ferrabini, A.T. Rios, C.T. Dutra: *Mater. Sci. Eng.*, 2006, vol. 435, pp. 139-144.
 10. M. Sireesha, Shaju K. Albert, V. Shankar, S. Sundaresan: *J. Nucl. Mater.*, 2000, vol. 279, pp. 65-76.
 11. Kou Sindo: *Welding Metallurgy*, 2nd ed., John Wiley & Sons Inc., Hoboken New Jersey, 2003, pp. 173-180.
 12. J.C. Lippold: *Weld. J.*, 1983, vol. 62, pp. 1s-11s.
 13. S.K. Albert, T.P.S. Gill, A.K. Tyagi, S.L. Mannan, S.D. Kulkarni, P. Rodriguez: *Weld. J.*, 1997, vol. 66, pp. 135s-142s.
 14. H.T. Lee, T.Y. Kuo: *Sci. Technol. Weld. Joining*, 1999, vol. 4, pp. 94-103.
 15. R.A. Page: *Corrosion*, 1983, vol. 39, pp. 409-421. □